PTEP

Prog. Theor. Exp. Phys. **2025** 103E03 (20 pages)
DOI: 10.1093/ptep/ptaf134

Hubble Constant, S_8, and Sound Horizon Tensions: A Study Within the Teleparallel Framework

Sai Swagat Mishra * and P. K. Sahoo †

Department of Mathematics, Birla Institute of Technology and Science, Pilani, Hyderabad Campus, Jawahar Nagar, Kapra Mandal, Medchal District, Telangana 500078, India

Received July 26, 2025; Revised September 6, 2025; Accepted September 10, 2025; Published September 26, 2025

Increasingly precise cosmological observations have revealed subtle yet persistent discrepancies, collectively known as *cosmological tensions*. Despite the success of the standard ΛCDM model in describing the evolution of the universe, growing tensions between early- and late-time cosmological observations, such as those involving the Hubble constant and matter clustering amplitude, suggest the potential need for new physics beyond the concordance model. In this work, we have analyzed the H_0, S_8, and r_d tensions within the teleparallel framework. To do so, we propose a model where the matter is minimally coupled as an inverse term with the torsion scalar. Our analysis demonstrates that the inverse torsion term primarily impacts the late-time expansion, shifting the inferred H_0, while the $\mathcal{T}$ coupling modifies structure growth, reducing the S_8 tension. Through joint analyses with DESI, GW, CC, and Union3 data, we show that this $f(T, \mathcal{T})$ model can statistically compete with ΛCDM ($\Delta\chi^2 \lesssim 2$), while offering distinct physical insights into the origin of the observed cosmological tensions. Our findings not only shed light on the possible alleviation of existing cosmological tensions but also reinforce the consistency of the universe's late-time accelerated expansion and its dynamical transition history.

Subject Index E03, E60, E64, E65, E74

1. Introduction

The most profound revelation in modern cosmology is the discovery of the late-time acceleration of the universe. Some prominent observational evidence, most notably from Type Ia supernovae [1,2], the cosmic microwave background (CMB) [3,4], and baryon acoustic oscillations (BAO) [5,6], has firmly established the fact that the expansion of the universe is not slowing down, as once expected, but is instead accelerating. This unexpected behavior, occurring long after the radiation- and matter-dominated eras, challenges our understanding of gravity and the energy content of the cosmos. Within the framework of general relativity (GR), this acceleration is typically attributed to a mysterious component known as dark energy, which contributes a dominant and repulsive effect on cosmic scales. The nature, origin, and dynamics of this component remain central questions in theoretical physics and cosmology today.

Among many theoretical frameworks, the Lambda cold dark matter (ΛCDM) model has emerged as the most widely accepted. The cosmological constant Λ is interpreted as a form of vacuum energy with constant energy density and negative pressure, responsible for the accelerated expansion. Despite being very successful in fitting the wide range of observations, the model is lacking in some contexts. One of the major drawbacks is the *cosmological tensions*.

*saiswagat009@gmail.com
†pksahoo@hyderabad.bits-pilani.ac.in

In cosmology, independent surveys are generally expected to produce compatible estimates of key parameters within statistical uncertainties. However, when significant discrepancies emerge between the outcomes of well established observations, such inconsistencies are termed "tensions". If systematic errors are ruled out, these tensions prompt a closer examination of the foundational theoretical framework and may indicate the need for new physics. When it comes to the Hubble constant, the Planck results predict $H_0 \approx 67.4$ km/s/Mpc with ΛCDM as the underlying model. However, the model-independent measurements, such as SH0ES, suggest a significantly higher value $H_0 \approx 73$ km/s/Mpc. This mismatch exceeds the 5σ threshold and is no longer easily dismissed as a statistical fluke.

Another growing challenge to the ΛCDM model is the so-called S_8 *tension*, which refers to discrepancies in the measured amplitude of matter clustering in the universe. The parameter $S_8 \equiv \sigma_8\sqrt{\Omega_m/0.3}$ combines the matter density Ω_m and the root-mean-square fluctuation of matter σ_8 on $8\,h^{-1}$ Mpc scales. Measurements from the Planck satellite, assuming ΛCDM, predict a higher value of $S_8 \approx 0.83$, whereas *weak gravitational lensing surveys* such as KiDS, DES, and HSC report lower values around $S_8 \approx 0.76$, with discrepancies at the $\sim$2–3σ level. While not yet as statistically significant as the Hubble tension, the persistent nature of this mismatch across multiple independent surveys suggests potential cracks in the standard cosmological model. Proposed resolutions include systematic uncertainties in lensing data, but also theoretical extensions like modified gravity, interacting dark energy, or nonstandard neutrino physics, highlighting the need to scrutinize ΛCDM's assumptions and seek more flexible frameworks.

Together, the H_0 and S_8 tensions reflect a deeper inconsistency between early-universe and late-universe observations. This raises the possibility that a single underlying modification to the theory of gravity or cosmic components could address both anomalies simultaneously. These challenges have motivated a growing body of work exploring alternatives to general relativity and extensions of the ΛCDM framework, including scalar–tensor theories, dark sector interactions, and geometrically modified gravities such as teleparallel gravity.

To tackle these issues, we adopt the torsion-based geometrical modification of GR, known as the teleparallel equivalent of general relativity (TEGR) [7]. While the use of a curvature-free connection distinguishes TEGR from GR, both theories yield the same phenomenological predictions. Nevertheless, numerous studies in the literature highlight the importance and relevance of this alternative formulation [8–14]. In this work, we consider a specific class of extensions to the TEGR, namely the $f(T,\mathcal{T})$ gravity [15] framework, where T denotes the torsion scalar and $\mathcal{T} \equiv T^{\mu}_{\ \mu}$ is the trace of the energy–momentum tensor. This model generalizes standard $f(T)$ gravity by introducing a nonminimal coupling between torsion and matter, thereby allowing for richer cosmological dynamics and potential explanations for the late-time acceleration of the universe without invoking dark energy explicitly. The inclusion of $\mathcal{T}$ captures possible interactions between geometry and matter, offering a broader theoretical landscape to investigate deviations from general relativity and address existing observational tensions. Some interesting work on the theory can be found in Refs. [16–22].

The article is divided as follows. A brief background and perturbation level description of the $f(T,\mathcal{T})$ theory is presented in Section 2, followed by the mathematical formulation with a specific model choice in Section 3. Section 4 is dedicated to discussing the observational datasets. Afterwards, we analyze the impact of the results in various contexts in Section 5. The review of the existing tensions and the perspective of our model on that is discussed in Section 6. Finally, we conclude the results in Section 7.

2. Fundamentals of the theory

2.1. *Background level equations*

We commence by discussing the geometric foundation of the teleparallel equivalent of general relativity (TEGR) and its generalizations. On a differentiable manifold, the tangent space at any point x^α is spanned by a set of orthonormal tetrads $e_A(x^\alpha)$, satisfying the relations

$$dx^\alpha = e_A{}^\alpha \, \sigma^A, \quad \sigma^A = e^A{}_\alpha \, dx^\alpha. \tag{1}$$

Using this, the spacetime line element becomes

$$ds^2 = g_{\alpha\beta} \, dx^\alpha dx^\beta = \eta_{AB} \, \sigma^A \sigma^B, \tag{2}$$

where $\eta_{AB} = \mathrm{diag}(+1, -1, -1, -1)$ is the Minkowski metric, and the tetrads satisfy the orthonormality conditions

$$e_A{}^\alpha \, e^A{}_\beta = \delta^\alpha_\beta, \quad e_A{}^\alpha \, e^B{}_\alpha = \delta^B_A. \tag{3}$$

It is well known that the TEGR formalism uses the Weitzenböck connection, instead of the usual Levi–Civita connection of GR. The connection reads

$$\overset{w}{\Gamma}{}^A{}_{\alpha\beta} \equiv e_B{}^A \partial_\beta e^B{}_\alpha = -e^B{}_\alpha \partial_\beta e_B{}^A. \tag{4}$$

The Weitzenböck connection is not symmetric in its lower indices, which gives rise to a nonzero torsion tensor,

$$T^A{}_{\alpha\beta} = \overset{w}{\Gamma}{}^A{}_{\alpha\beta} - \overset{w}{\Gamma}{}^A{}_{\beta\alpha}. \tag{5}$$

Further, the contorsion tensor, which is different between the Weitzenböck and Levi–Civita connections, is defined as

$$K^{\alpha\beta}{}_A = \overset{w}{\Gamma}{}^A{}_{\alpha\beta} - \Gamma^A{}_{\alpha\beta} = -\frac{1}{2}\left(T^{\alpha\beta}{}_A - T^{\beta\alpha}{}_A - T_A{}^{\alpha\beta}\right). \tag{6}$$

With the help of the superpotential tensor, the torsion scalar, one of the most important quantities, is defined as

$$T \equiv S_A{}^{\alpha\beta} T^A{}_{\alpha\beta} = \frac{1}{4} T^{A\alpha\beta} T_{A\alpha\beta} + \frac{1}{2} T^{A\alpha\beta} T_{\beta\alpha A} - T_{A\alpha}{}^A T^{\beta\alpha}{}_\beta. \tag{7}$$

The TEGR gravitational action can be defined as

$$S_{\mathrm{TEGR}} = \frac{1}{2k^2} \int d^4x e \; T + \int d^4x e \mathcal{L}_m, \tag{8}$$

where $k = \sqrt{8\pi G}$, $e = \sqrt{-g}$, and $\mathcal{L}_m$ represents the matter Lagrangian. Similar to how GR can be extended through the $f(R)$ theory, where the Ricci scalar R is replaced with a general function $f(R)$, the TEGR can also be generalized by promoting the torsion scalar T to a function $f(T)$. However, due to the nonlinear contribution of the boundary term, the resulting $f(T)$ theory is no longer dynamically equivalent to $f(R)$ gravity. In this study, we consider a further generalization of $f(T)$ gravity involving a coupling between the torsion scalar T and the trace of the energy–momentum tensor $\mathcal{T}$, known as $f(T, \mathcal{T})$ gravity (introduced in Ref. [15]). The action for this theory is given by [23,24]:

$$S_{f(T,\mathcal{T})} = \frac{1}{2k^2} \int d^4x e \left[T + f(T, \mathcal{T})\right] + \int d^4x e \mathcal{L}_m. \tag{9}$$

It is very evident that the TEGR action can be recovered with the generalized functional form $f(T, \mathcal{T})$ being zero. Varying the action with respect to the vierbeins leads to the field

equation [17]

$$2(1+f_T)\left[e^{-1}\partial_\alpha(e\,e_B{}^A S_A^{\gamma\alpha}) - e_B^A T^\alpha_{\beta A} S_\alpha^{\beta\gamma}\right] + 2\left(f_{TT}\,\partial_\alpha T + f_{T\mathcal{T}}\,\partial_\alpha \mathcal{T}\right) e\, e_B^A S_A^{\gamma\alpha} + e_B^\gamma \left(\frac{f+T}{2}\right)$$
$$-f_{\mathcal{T}}\left(e_B^A \overset{\text{em}}{T}{}_A^{\ \gamma} + p\, e_B^\gamma\right) = k^2\, e_B^A \overset{\text{em}}{T}{}_A^{\ \gamma}\,. \tag{10}$$

Here, f denotes the functional of both variables T and $\mathcal{T}$ and $\overset{\text{em}}{T}{}_A^{\ \gamma}$ is the energy–momentum tensor. From now on, we consider a spatially flat Friedmann–Lemaître–Robertson–Walker (FLRW) metric of the form

$$ds^2 = dt^2 - a^2(t)(dx^2 + dy^2 + dz^2), \tag{11}$$

with $a(t)$ being the scale factor in terms of cosmic time. For this metric, the vierbein field is of the form $e_A{}^\alpha = \text{diag}(1, a, a, a)$. With this choice of metric, a formal relation between the torsion scalar and Hubble parameter ($H(t) = \frac{\dot{a}(t)}{a(t)}$) comes up as

$$T(t) = -6H^2(t). \tag{12}$$

Finally, we note down the two motion equations that come from the field equation (10) and line element (11),

$$3H^2 = k^2\rho_m - \frac{1}{2}(f + 12H^2 f_T) + f_{\mathcal{T}}(\rho_m + p_m), \tag{13}$$

$$2\dot{H} = -k^2(\rho_m + p_m) - 2\dot{H}(f_T - 12H^2 f_{TT}) - 2H(\dot{\rho_m} - 3\dot{p_m})f_{T\mathcal{T}} - f_{\mathcal{T}}(\rho_m + p_m). \tag{14}$$

Analogous to GR, with the convention $k = 1$, one can rewrite the motion equations as

$$3H^2 = \rho_m + \rho_{\text{DE}}, \tag{15}$$

$$-2\dot{H} = \rho_m + p_m + \rho_{\text{DE}} + p_{\text{DE}}, \tag{16}$$

where

$$\rho_{\text{DE}} = -6H^2 f_T + f_{\mathcal{T}}(\rho_m + p_m) - \frac{f}{2}, \tag{17}$$

$$p_{\text{DE}} = (6H^2 + 2\dot{H})f_T + \frac{f}{2} - 24H^2\dot{H} f_{TT} + 2H(\dot{\rho}_m - 3\dot{p}_m)f_{T\mathcal{T}}. \tag{18}$$

To study the evolution of the universe, the effective equation of state (EoS) parameter plays a very significant role. The definition of the total EoS parameter is

$$w_{\text{tot}} = \frac{p_{\text{tot}}}{\rho_{\text{tot}}} = \frac{p_m + p_{\text{DE}}}{\rho_m + \rho_{\text{DE}}}. \tag{19}$$

The deceleration parameter predicts the phase transitional behavior and the late-time acceleration of the universe. It reads

$$q(t) = -\frac{1}{a(t)H^2(t)}\frac{d^2a(t)}{dt^2}. \tag{20}$$

It is well established that generic extensions of teleparallel gravity, such as $f(T)$ or $f(T, \mathcal{T})$ models, formulated in the pure tetrad approach are not locally Lorentz invariant. A covariant formulation with an appropriate spin connection has been proposed in the literature [25] to systematically restore covariance and ensure consistency at the theoretical level. In the present work, our interest lies in the phenomenological implications of the proposed model for cosmology. Since we work with the proper diagonal FLRW tetrad, often referred to as a "good tetrad", the cosmological background equations remain unaffected by Lorentz invariance issues. Thus,

our analysis of the background evolution and cosmological tensions is self-consistent within this setting. Nevertheless, it would be interesting in future work to reexamine the model in the fully covariant teleparallel framework in order to test the robustness of our conclusions beyond the FLRW background.

2.2. *Perturbation level equations*

The growth rate of matter perturbation is defined as

$$f(a) \equiv \frac{dln\delta_m(a)}{da}, \tag{21}$$

and the root-mean-square mass fluctuation reads

$$\sigma_8(a) = \sigma_{8,0}\frac{\delta_m(a)}{\delta_{m0}}, \tag{22}$$

where δ_m is the matter density perturbation and $\sigma_{8,0}$ is the present value of σ_8. The product of these two quantities gives rise to $f\sigma_8$, which is the observable quantity. Most measurements of the growth rate of cosmic structures have been reported in terms of the combined parameter since around 2006. The structure growth parameter S_8 can be defined as

$$S_8 = \sigma_8\sqrt{\frac{\Omega_{m0}}{0.3}}. \tag{23}$$

Within the subhorizon limit, the dynamics of matter perturbations in $f(T, \mathcal{T})$ gravity are described by the following differential equation:

$$\delta_m{}''(a) + \left(\frac{H'(a)}{H(a)} + \frac{3}{a}\right)\delta_m{}'(a) = \frac{3}{4}\frac{\Omega_m G_{\rm eff}}{a^2}\left(\frac{H_0}{H(a)}\right)^2\delta_m(a), \tag{24}$$

where $G_{\rm eff}$ is Newton's constant. By solving the above differential equation, and applying the solution to Eqs. (21) and (22), one can achieve the theoretical form of $f\sigma_8$.

Next, we proceed with a particular choice of functional form of the theory and its cosmological implications in the upcoming sections.

3. Mathematical formulation

We consider the functional form

$$f(T, \mathcal{T}) = \frac{aT_0^2}{T} + b\mathcal{T}, \tag{25}$$

where a and b are dimensionless free model parameters. The model is chosen because of its hybrid nature; specifically, the presence of the H^2 term in both numerator ($\mathcal{T} = \rho_m \sim H^2$) and denominator makes it viable to explain both early- and late-time scenarios. These features of this class of models can be seen in Ref. [26]. In addition, in Ref. [27], the model has shown its suitability to explain the tensions. We have extended it with the inclusion of the trace of the energy–momentum tensor term. Employing this model in the first Friedmann equation (13) gives rise to

$$H^2(z) = \frac{\rho_{m0}}{6}(2+b)(1+z)^3 + \frac{3aH_0{}^4}{H^2(z)}. \tag{26}$$

Here H_0 and ρ_{m0} are the present time ($z = 0$) Hubble parameter and matter density, respectively. Model parameter dependence can be achieved conveniently by assuming the present scenario in the above equation. It is

$$a = \frac{1}{3}\left(1 - \frac{\Omega_{m0}}{2}(2+b)\right). \tag{27}$$

The relation $\rho_{m0} = 3\Omega_{m0}H_0{}^2$ is applied in the above equation, where Ω_{m0} is the present matter density parameter. Now, our Hubble expression remains with the cosmological parameters along with an additional parameter b.

Although the functional form in Eq. (25) appears simple, it is not without theoretical motivation. The inclusion of $\mathcal{T}$ is the teleparallel analog of the $f(R, \mathcal{T})$ framework [28]. A stability analysis was already carried out in the original work [15], showing that such couplings can lead to consistent and viable cosmological dynamics. The inverse torsion contribution is motivated by infrared modifications of gravity, analogous to inverse-R terms in $f(R)$ models [29,30], which are known to generate late-time acceleration without an explicit cosmological constant. Moreover, the foundational work on $f(T, \mathcal{T})$ theory [15] has shown, via both background dynamics and linear perturbation analysis, that a wide class of $f(T, \mathcal{T})$ models can be free of ghosts and instabilities while allowing for a consistent cosmological evolution across matter-dominated and accelerated epochs [16,18,24]. Therefore, our model should not be seen as a naive Ansatz but as a phenomenologically grounded extension of teleparallel gravity with precedents in the literature. It is worth noting that, in general, this theory does not guarantee the standard conservation law $\nabla_\mu T^{\mu\nu} = 0$ due to the nonminimal matter–torsion coupling. However, for linear or constant dependence on $\mathcal{T}$, the conservation is preserved [18]. Since our model contains only a linear $\mathcal{T}$ term, energy–momentum conservation holds in the present case.

To further investigate the cosmological implications of this model, we make use of the Markov chain Monte Carlo (MCMC) statistical technique. The next section presents some fundamental understanding of the concerned datasets along with the methodology.

4. Observational constraints and methodology

To constrain the free parameters of our model, we perform a Bayesian statistical analysis using the MCMC technique. The Bayesian framework is based on Bayes' theorem,

$$\mathcal{P}(\mathbf{\Theta}|\mathcal{D}) = \frac{\mathcal{L}(\mathcal{D}|\mathbf{\Theta})\,\pi(\mathbf{\Theta})}{\mathcal{Z}(\mathcal{D})}, \tag{28}$$

where $\mathbf{\Theta}$ denotes the set of model parameters, $\mathcal{D}$ the observational data, $\pi(\mathbf{\Theta})$ the prior distribution, $\mathcal{L}(\mathcal{D}|\mathbf{\Theta})$ the likelihood function, and $\mathcal{Z}(\mathcal{D})$ the Bayesian evidence (a normalization constant).

The likelihood function is expressed in terms of a χ^2 statistic as

$$\mathcal{L}(\mathcal{D}|\mathbf{\Theta}) \propto \exp\left[-\frac{1}{2}\chi^2(\mathbf{\Theta})\right], \tag{29}$$

with

$$\chi^2(\mathbf{\Theta}) = \sum_{i=1}^{N} \frac{\left[\mathcal{O}^{\rm th}(z_i, \mathbf{\Theta}) - \mathcal{O}^{\rm obs}(z_i)\right]^2}{\sigma_i^2}, \tag{30}$$

where $\mathcal{O}^{\rm th}$ and $\mathcal{O}^{\rm obs}$ denote the theoretical and observed values of an observable (e.g. $H(z)$, $D_A(z)$, $\mu(z)$), σ_i is the observational error, and N is the number of data points. The choice of priors $\pi(\mathbf{\Theta})$ reflects physically motivated ranges for the cosmological parameters and ensures that the sampling process remains statistically well behaved. This methodology is common to all the observational probes considered in this work.

The novelty of the present work lies in applying these formulations to the hybrid model and constraining it with a comprehensive set of the latest observations. In particular, we include the DESI first-year baryon acoustic oscillation measurements, gravitational-wave standard sirens,

recent cosmic chronometer (CC) determinations of the Hubble parameter, and the Union3 Type Ia supernova compilation. To the best of our knowledge, this is the first joint likelihood analysis in $f(T, \mathcal{T})$ gravity that considers this combination of datasets, thereby providing new insights into the H_0, S_8, and r_d tensions. In the following, we summarize the individual datasets employed in our analysis.

4.1. *DESI BAO*

The DESI BAO data from Data Release 1 include 12 measurements in the redshift range $0.1 < z < 4.2$ (refer to table 1 of Ref. [31]). The BAO analysis measures cosmological quantities in each redshift bin as either two correlated distance ratios, $\frac{D_M}{r_d}$ and $\frac{D_H}{r_d}$, or a single ratio, $\frac{D_V}{r_d}$, depending on the signal-to-noise ratio. BAO measurements rely on the sound horizon at the drag epoch, r_d, which represents the distance that sound waves could travel from the Big Bang until the drag epoch, the time when baryons decoupled from photons. The definition of r_d reads

$$r_d = \frac{1}{H_0} \int_{z_d}^{\infty} \frac{c_s(z^*)}{E(z^*)} dz^*. \tag{31}$$

Further, the other distance-measuring functions are defined as

$$D_M(z) = \frac{c}{H_0} \int_0^z \frac{dz^*}{E(z^*)}, \tag{32}$$

$$D_H(z) = \frac{c}{H(z)}, \tag{33}$$

$$D_V(z) = \left[z\, D_H(z)\, D_M{}^2(z) \right]^{\frac{1}{3}}, \tag{34}$$

where $E(z) = H(z)/H_0$ is the normalized Hubble parameter, and c and c_s represent the speed of light and the fluid sound of baryon–photons, respectively. The compilation of the samples achieved from different redshift ranges is distinguished by the tracers. The tracers are from four classes of extragalactic targets, namely, the bright galaxy sample (BGS), luminous red galaxies (LRG), emission line galaxies (ELG), and quasars (QSO). Additionally, the Lyman-α forest sample (Lyα) traces the spectra of high-redshift quasars ($1.77 < z < 4.16$). For additional information on the DESI DR1 BAO measurements, see Ref. [31].

4.2. *Redshift space distortion*

To study the S_8 tension, the growth rate data, also known as redshift space distortion (RSD) data, play a very significant role. The compilation contains the observation value of $f\sigma_8(a)$ from different surveys like WiggleZ, eBOSS, etc. The complete table of the compilation can be found in Table II of Ref. [32]. These data are commonly referred to in the literature as RSD data, due to a specific phenomenon observed at both large and small scales during galaxy observations. In essence, the peculiar velocities of galaxies cause overdense regions to appear compressed along the line of sight at large scales, while at small scales, these regions become elongated along the line of sight. This distortion affects the two-point correlation function, leading to an anisotropic distribution in the power spectrum.

Additionally, at large scales, part of the observed anisotropy in the power spectrum may also stem from using an incorrect fiducial cosmology for $H(z)$, an effect known as the Alcock–Paczynski (AP) effect. This factor must be considered when analyzing growth rate data. The

AP effect causes a correction [33] that can be approximated as [34]

$$f\sigma_8(a) \approx \frac{H(a)D_A(a)}{\tilde{H}(a)\tilde{D}_A(a)}\tilde{f}\sigma_8(a). \tag{35}$$

Here, $H(a)$ and $D_A(a)$ represent the Hubble parameter and the angular diameter distance for the cosmological model under investigation, while $\tilde{H}(a)$ and $\tilde{D}_A(a)$ denote the corresponding quantities in the fiducial cosmology used for data analysis. The quantity $f\sigma_8(a)$ represents the reference value provided by the data, which requires correction to account for the differences between the fiducial and target cosmological models.

4.3. *Gravitational waves*

The recent observation of gravitational waves (GWs) from compact binary mergers by LIGO–Virgo [35] has introduced new challenges for modified gravity theories. Within these frameworks, tensor perturbation equations are expected to be altered, which in turn affects the propagation of GWs. A useful approach to quantify such deviations is through the analysis of the gravitational-wave luminosity distance. Gravitational waves generated by inspiraling binary systems, such as black hole binaries (BH–BH), neutron star binaries (NS–NS), or neutron star–black hole (NS–BH) pairs, can function as "standard sirens", enabling direct determination of luminosity distances without relying on the conventional cosmic distance ladder.

In this work, we utilize the gravitational-wave (GW) data from the Gravitational-Wave Transient Catalog (GWTC). This catalog contains detections from the LIGO, Virgo, and KAGRA Collaborations. From different observing runs, GWTC-1 [36], GWTC-2 [37], GWTC-2.1 [38], and GWTC-3 [39] of compact binary coalescences are observed. Our analysis considers the 130 GW luminosity distance within the redshift range $0.01 < z < 0.9$.

4.4. *Cosmic chronometers*

The cosmic chronometer (CC) approach offers a direct method to determine the Hubble parameter $H(z)$ by examining the age differences of the oldest and most passively evolving galaxies across nearby redshifts. Originally proposed in Ref. [40], this technique relies exclusively on the absolute age measurements of stars within the Milky Way and the location of the first acoustic peak in the CMB angular power spectrum to place constraints on the redshift-averaged dark energy equation of state parameter, w. Their analysis indicates a value of $w < -0.8$ at the 68% confidence level. Furthermore, by evaluating dz/dt near $z \sim 0$ using data from the Sloan Digital Sky Survey (SDSS), they derived an independent estimation of the Hubble constant.

Expanding on this methodology, Ref. [41] imposed strong constraints on the Hubble parameter $H(z)$ over the redshift interval $0.15 < z < 1.1$ by examining the differential spectroscopic aging of early-type galaxies. The study utilized a dataset of approximately 11 000 early-type galaxies gathered from multiple spectroscopic surveys, spanning nearly 8 billion years of cosmic history ($0.15 < z < 1.42$). This analysis yielded eight new measurements of $H(z)$, with an accuracy ranging between 5% and 12% up to $z \sim 1.1$. Additionally, four more $H(z)$ measurements, based on a sample of 17 832 luminous red galaxies from the SDSS DR7 in the redshift range $0 < z < 0.4$, were reported in Ref. [42].

The work presented in Ref. [43] offers improved estimates of the cosmic expansion history by utilizing red-envelope galaxies. High-resolution spectra were obtained from 24 galaxy clusters in the redshift interval $0.2 < z < 1.0$ using the Keck LRIS spectrograph. These observations were supplemented with publicly available archival data from the SPICES and VVDS surveys.

This study builds on and enhances earlier measurements of the expansion history, particularly advancing the results of Ref. [44] by introducing two additional determinations. Several other important contributions used in this analysis can be found in Refs. [21,45–47]. In this work, we used 15 correlated CC data points from Ref. [48], while the remaining uncorrelated points were incorporated using the respective chi-squared formulations.

4.5. *Union3*

The Union3 supernova compilation is an extensive collection of 2087 Type Ia supernovae drawn from 24 different data samples, covering a redshift range of 0.01 to 2.26. These supernovae have been standardized to a uniform distance scale using the SALT3 light-curve fitting method. The dataset has been analyzed and binned using the UNITY1.5 Bayesian statistical framework. A set of 22 binned distance measurements from the Union3 dataset is presented in Ref. [49].

5. Interpretations

The extended teleparallel theory has been constrained using MCMC with a different set of combinations of local and early-universe datasets. The Hubble expression (26) plays the key role in finding the theoretical predictions in each case. Though some datasets do not directly predict the observational value of Hubble, the theoretical counterpart of the cosmological quantities that they predict can be easily achieved using Eq. (26). The 2D contours up to the 2σ confidence level are presented in Fig. 1. As the cosmological parameters have already been observed through various methods in the literature, it is easy to compare the results. In that context, our aim is to explore the long-standing tensions. The upcoming section is completely dedicated to discussing the existing tensions in the literature and our model's perspective on that. The precise numerical values up to 1σ can be found in Table 1. The negative correlation between H_0 and Ω_{m0} indicates that as the Hubble value increases, the matter density parameter decreases. In fact, our model parameter b shows a similar kind of relation with Ω_{m0}.

Further, the resulting values are examined against the datasets by plotting the cosmological entities. In all of those analyses, we have also included the famous ΛCDM model for comparison purposes. In Fig. 2, one can see that the Hubble parameter for all combinations fits the 34 error bars of the CC data and the standard cosmological model. The deceleration parameters in Fig. 3 show a transition of the universe from deceleration to the acceleration phase. The magnified region provides a clear image of the transition point (z_t) for each case. The present values of the deceleration parameter and the transition redshifts are summarized in Table 2. Another very interesting parameter is the equation of state (EoS), which predicts the evolution of the universe in each era. As for dark energy, the w value is constant throughout (i.e. -1); we have just plotted the cases of our model in Fig. 4. The value $-1 < w_{\rm tot} < -1/3$ indicates a quintessence-like behavior, while $w_{\rm tot} < -1$ indicates phantom-like behavior. The present values of our models lie in the quintessence region (see Table 2), confirming the late-time acceleration. For our model, the EoS and deceleration parameters are calculated using Eqs. (19) and (20), respectively.

Since gravitational-wave (GW) observations provide measurements of the luminosity distance, we compare the theoretical predictions with the observational data, including error bars, as shown in Fig. 5. The models demonstrate a good fit to the data, comparable to that of the ΛCDM model. A similar analysis is carried out for the Union3 supernova dataset, where we

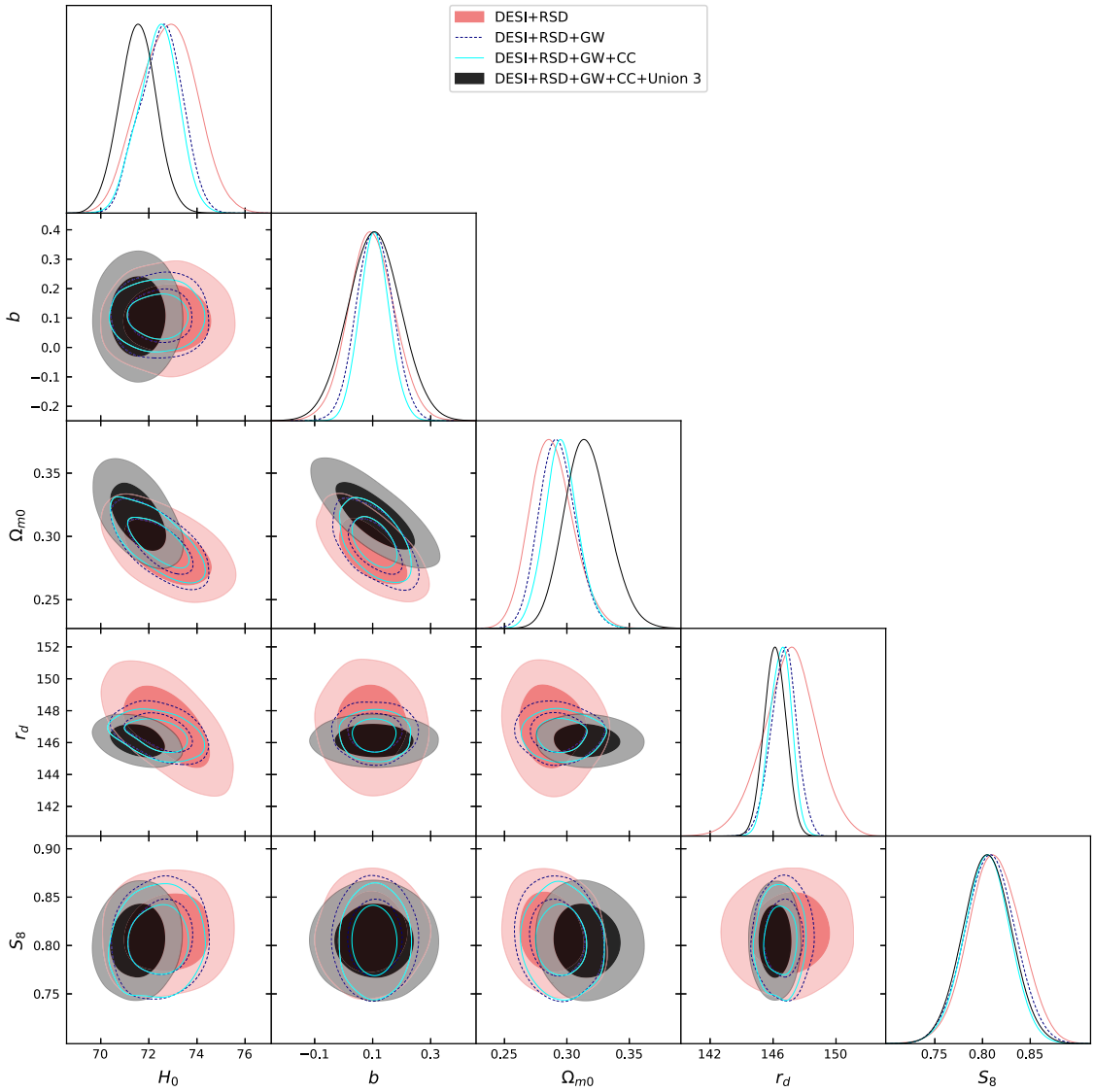

Fig. 1. 2D contours of the cosmological parameters up to the 2σ confidence level.

Table 1. Summary of the 1σ results obtained from MCMC for the $f(T, \mathcal{T})$ model.

Dataset	H_0 (km s^{-1} Mpc^{-1})	b	Ω_{m0}	r_d	S_8
DESI+RSD	72.8 ± 1.2	0.097 ± 0.079	$0.288^{+0.015}_{-0.019}$	147 ± 1.7	0.813 ± 0.027
DESI+RSD+GW	$72.51^{+0.95}_{-0.82}$	0.107 ± 0.061	$0.293^{+0.013}_{-0.015}$	146.66 ± 0.81	0.808 ± 0.026
DESI+RSD+GW+CC	$72.39^{+0.89}_{-0.76}$	0.107 ± 0.051	0.296 ± 0.014	146.47 ± 0.68	0.805 ± 0.024
DESI+RSD+GW+CC+Union3	71.54 ± 0.76	0.105 ± 0.091	$0.316^{+0.016}_{-0.019}$	146.13 ± 0.69	0.805 ± 0.025

compare the theoretical distance modulus with the observed values, incorporating the associated error bars. The results indicate that the models considered offer excellent agreement with the Union3 data (see Fig. 6), reinforcing their consistency with standard cosmological observations. In Fig. 7, we examine the behavior of the cases against the RSD data through f_{σ_8}. When plotted alongside the observational measurements and their uncertainties, the models show strong compatibility, effectively capturing the growth rate of cosmic structures across the redshift range. Finally, the distance-measuring functions involved in DESI BAO are compared.

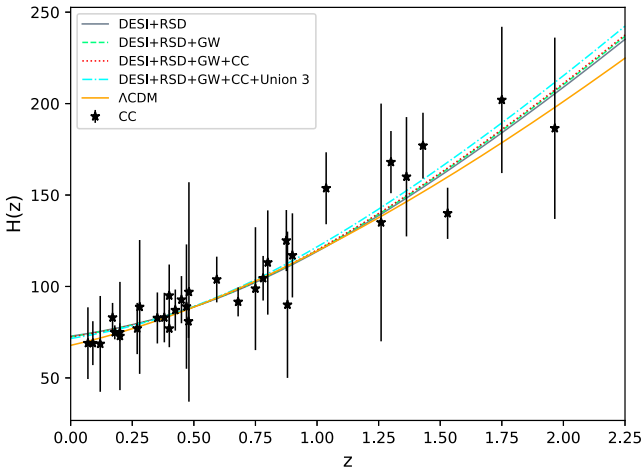

Fig. 2. Hubble parameter against redshift with 34 error bars of CC.

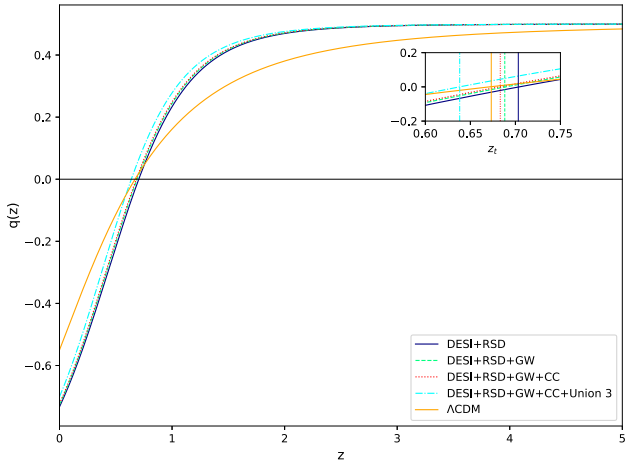

Fig. 3. Behavior of the deceleration parameter in the pre- and post-transitional eras with a magnified region of phase transition.

Table 2. Present values of the cosmological parameters.

Combinations	q_0	z_t	w_{tot_0}
DESI+RSD	−0.73	0.70	−0.82
DESI+RSD+GW	−0.72	0.68	−0.81
DESI+RSD+GW+CC	−0.72	0.68	−0.81
DESI+RSD+GW+CC+Union3	−0.70	0.63	−0.80
ΛCDM	−0.55	0.67	−1

The anisotropic and isotropic measurements are presented separately in Fig. 8. A similar trend to ΛCDM can be observed in all scenarios. In order to assess the performance of the model against the concordance ΛCDM scenario, we have computed the minimum χ^2 values for all dataset combinations, as summarized in Table 3. The differences $\Delta\chi^2$ are found to be small (typically $\mathcal{O}(1)$), indicating that the proposed $f(T, \mathcal{T})$ extension achieves a fit to current data that is statistically comparable to ΛCDM, thereby showing that it does not deteriorate the concordance with current observations.

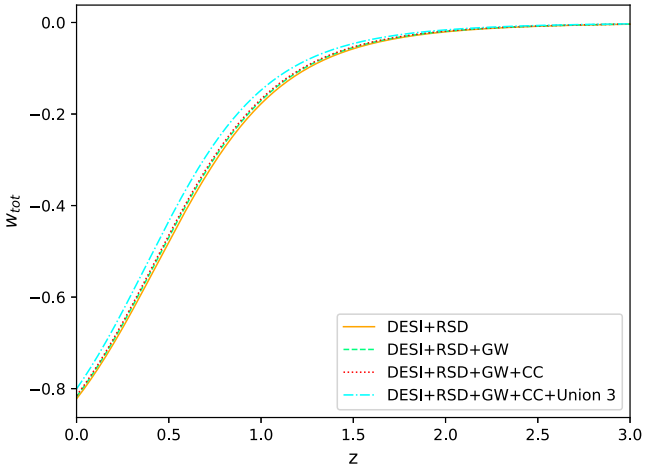

Fig. 4. Total equation of state parameter vs redshift.

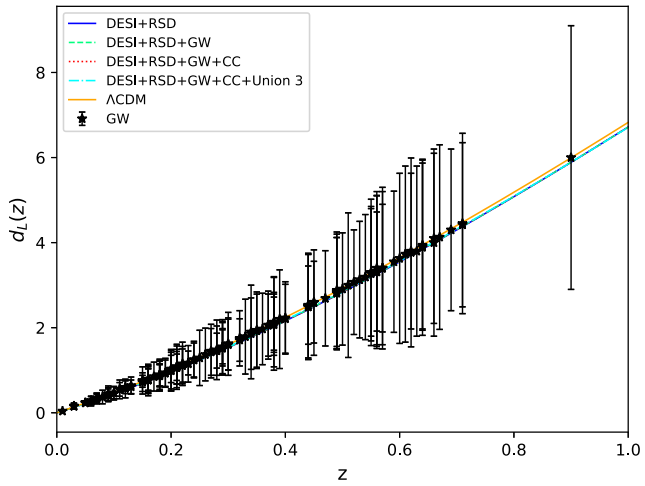

Fig. 5. Luminosity distance profile against redshift with GW data.

Having established the model's credibility through various observational comparisons in this section, we now turn our attention to the discussion of key cosmological tensions.

6. The tensions

Despite the remarkable success of the standard cosmological model in explaining a wide range of observations, several persistent tensions have emerged in recent years, challenging its completeness. Notably, discrepancies in the measurements of the Hubble constant H_0 and the matter fluctuation amplitude S_8 between early- and late-universe probes have attracted significant attention. These tensions are not only statistically significant but also potentially indicative of new physics beyond the ΛCDM paradigm. In this context, we explore how the teleparallel model addresses these anomalies and assess its effectiveness in alleviating or resolving the tensions by comparing it with the latest observations. Firstly, we report some major surveys and the discrepancies between them. Following that, how much our model fits/deviates from the landmark results will be discussed.

Beginning with the "gold standard" experimental result from the Planck 2018 observations under a flat ΛCDM framework, the Hubble constant is determined to be $H_0 = 67.27 \pm 0.60$

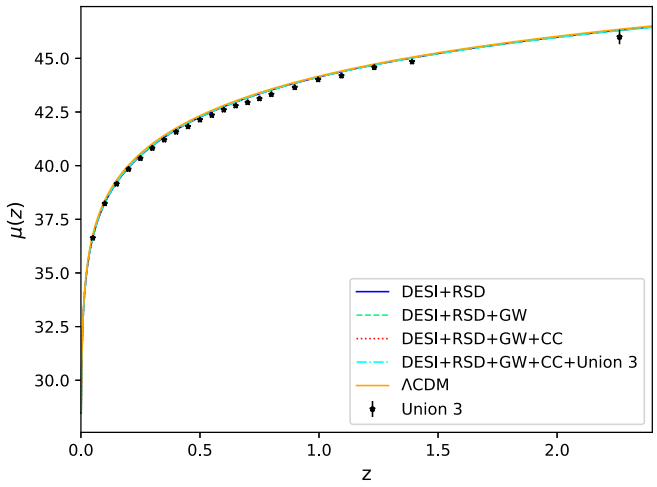

Fig. 6. Distance modulus profile against redshift with Union3 data.

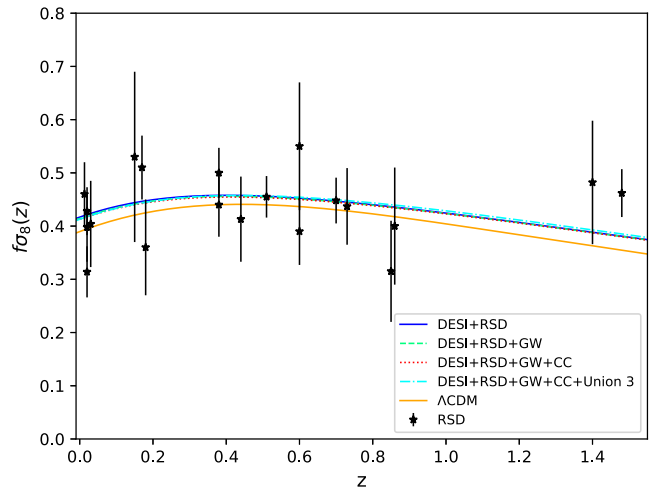

Fig. 7. Behavior of $f\sigma_8$ against redshift with error bars of RSD data.

km s^{-1} Mpc^{-1} at the 68% confidence level [4]. When four trispectrum measurements are incorporated into the Planck data, the value slightly shifts to $H_0 = 67.36 \pm 0.54$ km s^{-1} Mpc^{-1} for the combined Planck 2018+CMB lensing dataset [4]. The Hubble constant parameter measurement from the South Pole Telescope (SPT) Collaboration, as reported by Dutcher et al. [50], is $H_0 = 68.8 \pm 1.5$ km s^{-1} Mpc^{-1}. This measurement is independent of Planck observations and consistent with other CMB measurements. The H_0 measurement derived by D'Amico et al. [51] using BOSS DR12 data combined with Big Bang nucleosynthesis constraints, without relying on CMB, is $H_0 = 68.5 \pm 2.2$ km s^{-1} Mpc^{-1}. All the surveys that we have discussed so far are indirect measurements. Next, we will focus on some important direct measurements in the literature.

One of the most prominent model-independent direct measurement methods is the "distance ladder". It allows us to measure H_0 locally. By this method, the Type Ia supernovae (SNIa) Cepheid measurement, performed by the SH0ES team, reported the H_0 value 73.04 ± 1.04 km s^{-1} Mpc^{-1} at 68% CL [52]. A significant 5σ discrepancy between this measurement and that inferred from the CMB challenges the completeness of the standard cosmological model.

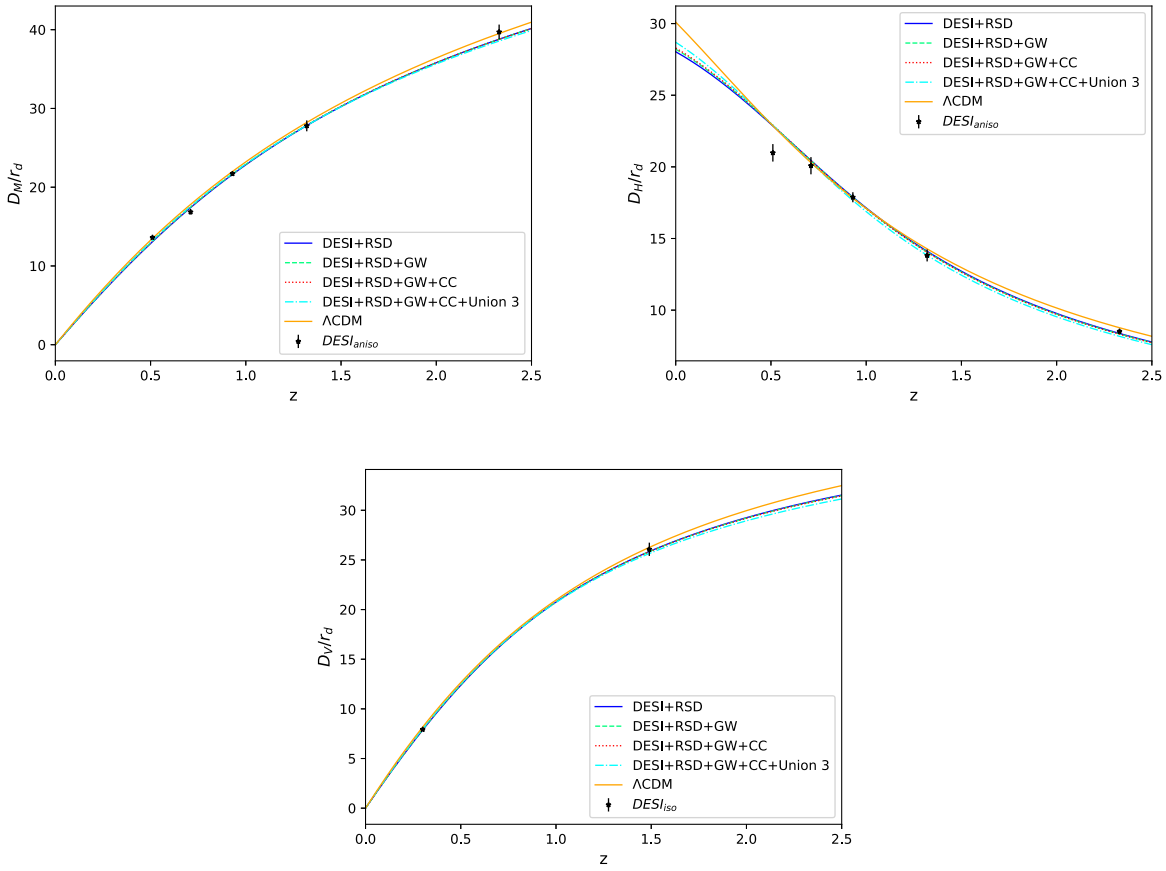

Fig. 8. The distance-measuring functions against redshift with DESI data.

Table 3. Comparison of the minimum χ^2 with the reference ΛCDM model.

Combinations	$\chi^2_{\rm min}$ (model)	$\chi^2_{\rm min}$ (ΛCDM)	$\Delta\chi^2$
DESI+RSD	33.27	32.06	1.21
DESI+RSD+GW	36.24	35.71	0.53
DESI+RSD+GW+CC	52.86	50.92	1.94
DESI+RSD+GW+CC+Union3	110.63	110.25	0.38

Using the tip of the red giant branch (TRGB) is another independent method to calculate H_0, which is based on the calibration of SNIa. With this method, Anand et al. [53] reported $H_0 = 71.5 \pm 1.8$ km s^{-1} Mpc^{-1} at 68% CL. The H II galaxy observations can serve as reliable distance indicators, independent of Type Ia supernovae, offering an alternative method to investigate the universe's background evolution. In Ref. [54], the authors' best estimate of the Hubble constant is $H_0 = 71.0 \pm 2.8\,(\text{random}) \pm 2.1\,(\text{systematic})\,\text{km s}^{-1}\,\text{Mpc}^{-1}$. The latest gravitational-wave standard-siren measurements have come up as revolutionary in the cosmological context. In Abbott et al. [39], the LIGO–Virgo–KAGRA Collaboration (GWTC-3) achieved $H_0 = 68^{+12}_{-7}$ km s^{-1} Mpc^{-1}. Further, the CC method (flat ΛCDM with systematics) [55] and TDCOSMO+SLACS [56] yield $H_0 = 66.5 \pm 5.4$ and $H_0 = 67.4^{+4.1}_{-3.2}$, respectively. Baxter et al. [57] combined CMB lensing measurements with supernova data to obtain the value $H_0 = 73.5 \pm 5.3$. This approach is notable because it does not rely on the sound horizon scale.

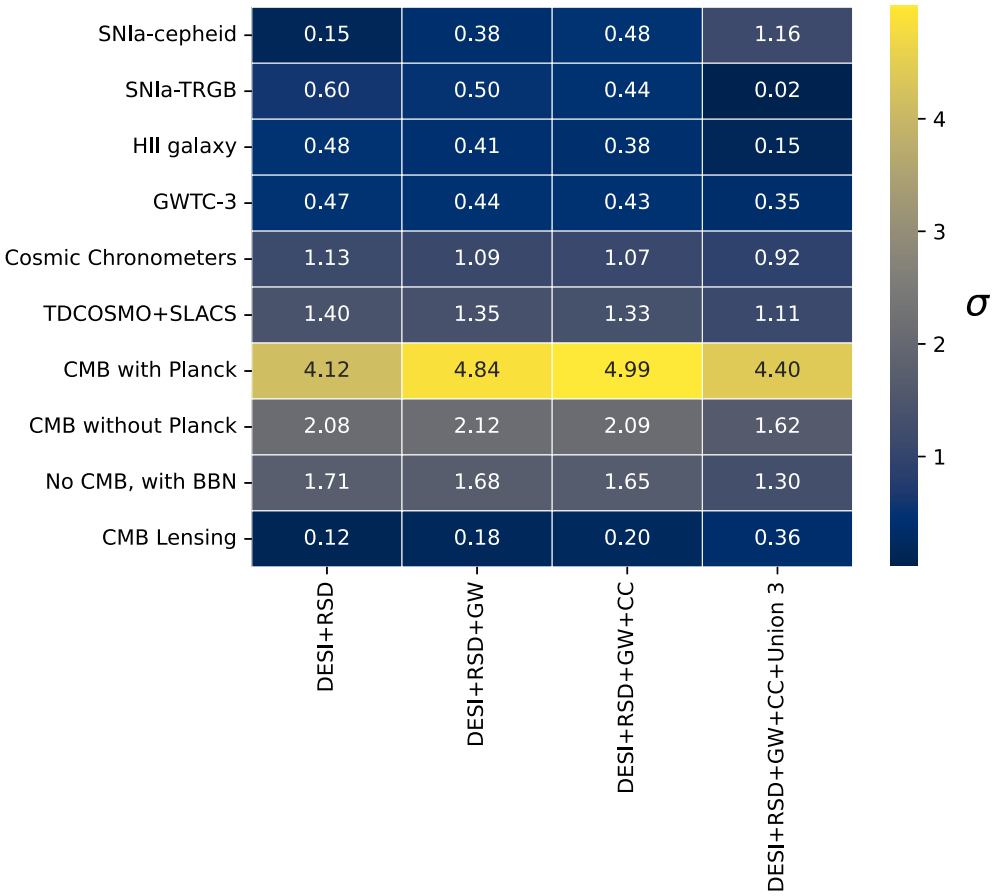

Fig. 9. Heat map of the H_0 tension between our combinations and various measurements.

The tension metric is used to calculate the deviation of our H_0 values from all these reviewed results. Figure 9 presents a heat map of σ between our model and the above-reviewed surveys. One can observe that for most of the observations, our model persists with 0–2σ tension, which indicates strong evidence in favour of the model. Though in the CMB with Planck, the tension is a little higher, it is reduced compared to the tension between Planck and SH0ES. In the first panel of Fig. 10, our results are compared against the Planck and SH0ES Collaborations.

A similar issue exists in the context of the matter fluctuation amplitude, known as S_8 tension. In particular, the results from the Planck satellite's measurements of the primary CMB anisotropies reveal a 2–3σ discrepancy in the amplitude of matter clustering compared to estimates from lower-redshift observations, such as weak gravitational lensing and galaxy clustering surveys. Here we note down some major findings from early-universe followed by late-universe surveys.

- Planck 2018 results (Aghanim et al. [4])
  - TT, TE, EE+LowE+Lensing+BAO: $S_8 = 0.825 \pm 0.011$
  - TT, TE, EE+LowE+Lensing: $S_8 = 0.832 \pm 0.013$
  - TT, TE, EE+LowE: $S_8 = 0.834 \pm 0.016$
- CMB ACT+WMAP: $S_8 = 0.84 \pm 0.011$ (Aiola et al. [58])
- WL KiDS-1000: $S_8 = 0.759 \pm 0.022$ (Asgari et al. [59])
- WL+GC DES-Y1: $S_8 = 0.773 \pm 0.023$ (Abbott et al. [60])

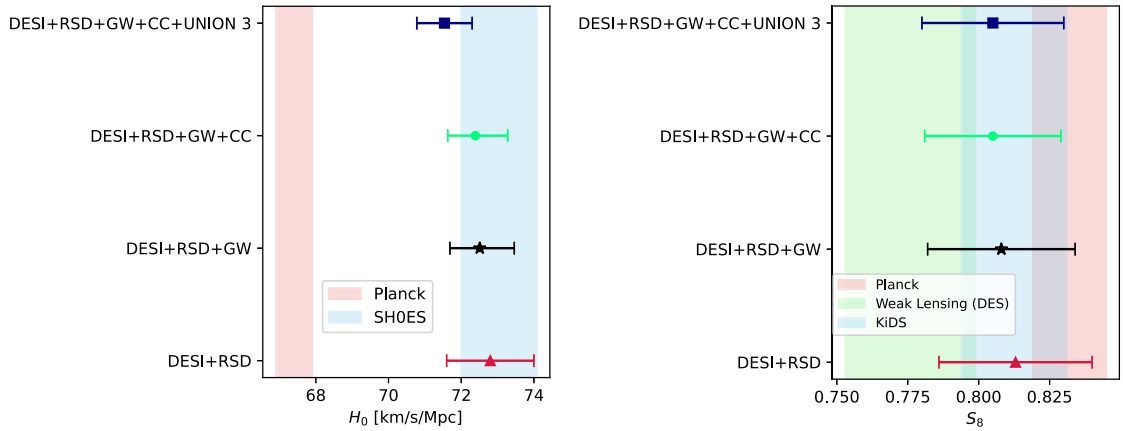

Fig. 10. Comparison of our results with the landmark early- and late-time surveys.

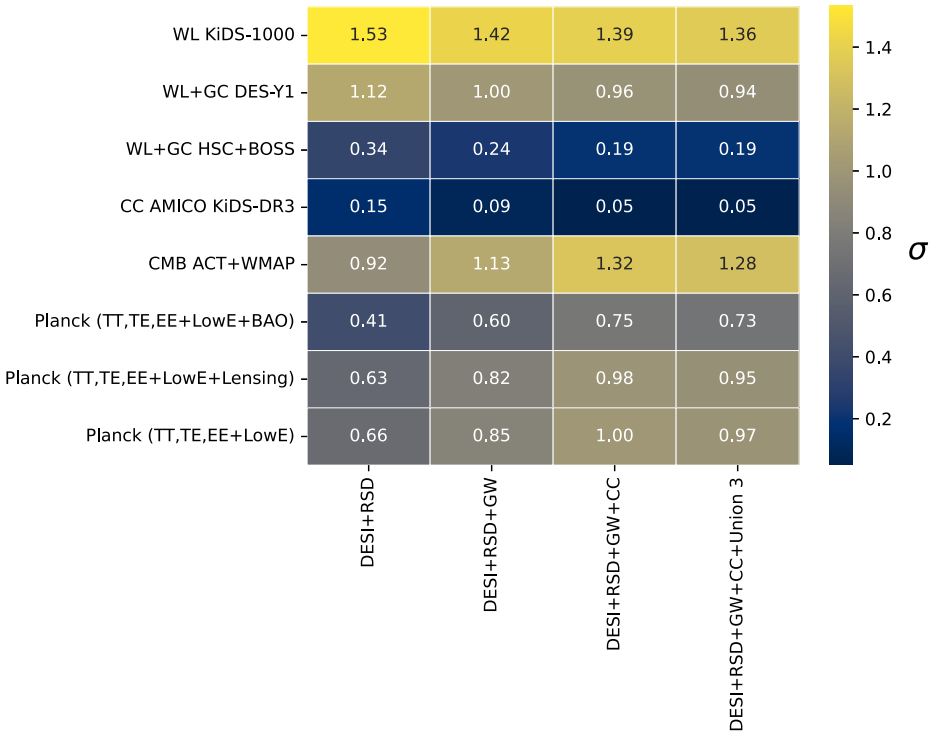

Fig. 11. Heat map of the S_8 tension between our combinations and various measurements.

- WL+GC HSC+BOSS: $S_8 = 0.795 \pm 0.045$ (Miyatake et al. [61])
- CC AMICO KiDS-DR3: $S_8 = 0.78 \pm 0.03$ (Lesci et al. [62])

Figure 11 represents a heat map of S_8 tension of our model with the aforementioned results. It is evident that our model has excellent agreement with both the early- and late-time surveys. The maximum observed tension is 1.5σ, while in the majority of cases it remains within 1σ. Also, the second panel of Fig. 10 demonstrates a clear visualization of the model's efficacy in alleviating the S_8 tension.

Finally, we explore the sound horizon at the drag epoch (r_d). It is well known that H_0 is negatively correlated with r_d. Even in our contours (Fig. 1), this behavior is observed. This is the

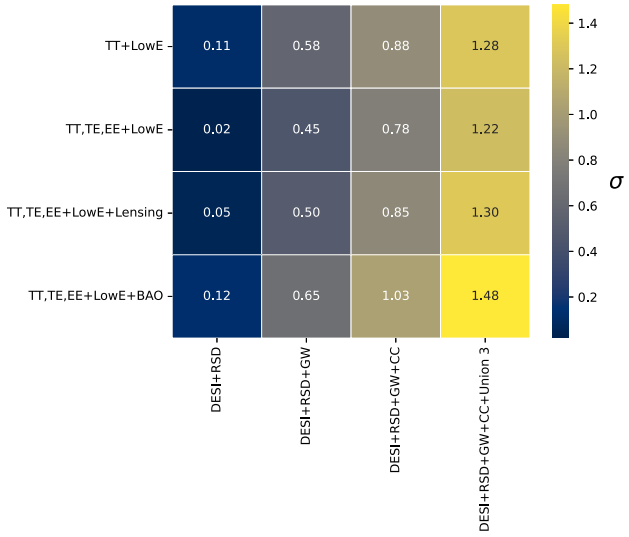

Fig. 12. Heat map of the r_d tension between our combinations and Planck measurements.

reason for which the late-time surveys with high H_0 predict a lower r_d compared to Planck. In particular, when the BAO surveys are combined with H_0-based measurements like H0LiCOW, SH0ES, and SNIa calibrations, they predict r_d around 135–140 Mpc. However, despite having higher H_0 values than the Planck results, our models produce suitable sound horizon values. To get a clear overview of this, we have compared our results with the four cases of the Planck results through a heat map in Fig. 12. For all the combinations, the tension is within 1.5σ, which confirms the model's excellence in resolving the sound horizon problem.

7. Concluding statements

In recent years, a variety of theoretical models have emerged with promising results that challenge the standard cosmological framework [27,63,64]. Although a definitive theory that resolves all the limitations of general relativity remains elusive, several modified gravity models have demonstrated significant promise in addressing specific cosmological challenges. In light of these developments, this work considered a torsion-based modification of gravity as a potential framework to address the cosmological tensions.

To constrain the parameters, we commence with the MCMC technique with a new set of combinations of datasets. The DESI BAO data is considered due to its strong constraining power. Combining RSD opens up the possibility to constrain and study the S_8 parameter. The latest GW observations have come up as very promising observations in the low-redshift paradigm. The CC method is very popular due to its differential aging technique. Finally, we have considered the recent supernova data, Union3.

Furthermore, the credibility of the obtained results is substantiated by examining the cosmic evolution. The model exhibits a smooth and consistent phase transition, as demonstrated by the behavior of the deceleration parameter. Its excellent fit to the observational datasets, along with consistency with the ΛCDM model, highlights its potential as a strong candidate for describing the late-time acceleration of the universe.

Finally, we observe that the model successfully alleviates the S_8 tension. The H_0 tension with Planck results is notably reduced, while it is effectively resolved when compared with other

observational surveys. Additionally, the derived sound horizon values show excellent agreement with those reported by the Planck results. The joint parameter space analysis shows that the model can shift the inferred values of H_0, S_8, and r_d toward alleviating the respective tensions. This is achieved through the combined action of the inverse torsion term, which influences background expansion, and the $\mathcal{T}$ coupling, which modifies the growth sector. As a future perspective, the proposed methodology can be applied to upcoming, more precise datasets, which may potentially lead to a complete resolution of the existing cosmological issues.

Acknowledgments

S.S.M. acknowledges the Council of Scientific and Industrial Research (CSIR), Government of India, for awarding a Junior Research Fellowship (E-Certificate No.: JUN21C05815). P.K.S. acknowledges the Anusandhan National Research Foundation (ANRF), Department of Science and Technology (DST), Government of India, for financial support to carry out Research Project No. CRG/2022/001847 and IUCAA, Pune, India, for providing support through the Visiting Associateship program. We are very grateful to the honorable referee and to the editor for the illuminating suggestions that have significantly improved our work in terms of research quality and presentation.

Data availability

There are no new data associated with this article.

REFERENCES

[1] A. G. Riess et al. [Supernova Search Team], Astron. J. **116**, 1009 (1998) [arXiv:astro-ph/9805201] [Search inSPIRE].
[2] S. Perlmutter et al. [Supernova Cosmology Project], Astrophys. J. **517**, 565 (1999) [arXiv:astro-ph/9812133] [Search inSPIRE].
[3] D. N. Spergel et al., Astrophys. J. Suppl. **148**, 175 (2003) [arXiv:astro-ph/0302209] [Search inSPIRE].
[4] N. Aghanim et al. [Planck Collaboration], Astron. Astrophys. **641**, A6 (2020); **652**, C4 (2021) [erratum][arXiv:1807.06209 [astro-ph.CO]] [Search inSPIRE].
[5] D. J. Eisenstein et al. [SDSS Collaboration], Astrophys. J. **633**, 560 (2005) [arXiv:astro-ph/0501171] [Search inSPIRE].
[6] L. Anderson et al. [BOSS Collaboration], Mon. Not. R. Astron. Soc. **441**, 24 (2014) [arXiv:1312.4877 [astro-ph.CO]] [Search inSPIRE].
[7] A. Unzicker and T. Case, arXiv:physics/0503046[Search inSPIRE].
[8] J. W. Maluf, J. F. da Rocha-Neto, T. M. L. Toribio, and K. H. Castello-Branco, Phys. Rev. D **65**, 124001 (2002) [arXiv:gr-qc/0204035] [Search inSPIRE].
[9] R. Ferraro and F. Fiorini, Phys. Rev. D **75**, 084031 (2007) [arXiv:gr-qc/0610067] [Search inSPIRE].
[10] E. V. Linder, Phys. Rev. D **81**, 127301 (2010); **82**, 109902 (2010) [erratum][arXiv:1005.3039 [astro-ph.CO]] [Search inSPIRE].
[11] P. Wu and H. W. Yu, Phys. Lett. B **693**, 415 (2010) [arXiv:1006.0674 [gr-qc]] [Search inSPIRE].
[12] J. B. Dent, S. Dutta, and E. N. Saridakis, J. Cosmol. Astropart. Phys. **1101**, 009 (2011) [arXiv:1010.2215 [astro-ph.CO]] [Search inSPIRE].
[13] G. Kofinas and E. N. Saridakis, Phys. Rev. D **90**, 084045 (2014) [arXiv:1408.0107 [gr-qc]] [Search inSPIRE].
[14] N. S. Kavya, S. S. Mishra, P. K. Sahoo, and V. Venkatesha, Mon. Not. R. Astron. Soc. **532**, 3126 (2024) [arXiv:2407.09589 [gr-qc]] [Search inSPIRE].
[15] T. Harko, F. S. N. Lobo, G. Otalora, and E. N. Saridakis, J. Cosmol. Astropart. Phys. **1412**, 021 (2014) [arXiv:1405.0519 [gr-qc]] [Search inSPIRE].
[16] D. Saez-Gomez, C. S. Carvalho, F. S. N. Lobo, and I. Tereno, Phys. Rev. D **94**, 024034 (2016) [arXiv:1603.09670 [gr-qc]] [Search inSPIRE].
[17] G. Farrugia and J. Levi Said, Phys. Rev. D **94**, 124004 (2016) [arXiv:1612.00974 [gr-qc]] [Search inSPIRE].

[18] E. L. B. Junior, M. E. Rodrigues, I. G. Salako, and M. J. S. Houndjo, Classical Quantum Gravity **33**, 125006 (2016) [arXiv:1501.00621 [gr-qc]] [Search inSPIRE].
[19] S. S. Mishra, S. Mandal, and P. K. Sahoo, Phys. Lett. B **842**, 137959 (2023) [arXiv:2305.09707 [gr-qc]] [Search inSPIRE].
[20] S. S. Mishra, A. Kolhatkar, and P. K. Sahoo, Phys. Lett. B **848**, 138391 (2024) [arXiv:2312.07558 [astro-ph.CO]] [Search inSPIRE].
[21] S. S. Mishra, N. S. Kavya, P. K. Sahoo, and V. Venkatesha, Astrophys. J. **970**, 57 (2024) [arXiv:2406.06661 [gr-qc]] [Search inSPIRE].
[22] S. Mandal, O. Sokoliuk, S. S. Mishra, and P. K. Sahoo, Nucl. Phys. B **993**, 116285 (2023) [arXiv:2301.06328 [astro-ph.CO]] [Search inSPIRE].
[23] M. G. Ganiou, I. G. Salako, M. J. S. Houndjo, and J. Tossa, Astrophys. Space Sci. **361**, 57 (2016) [arXiv:1512.04801 [physics.gen-ph]] [Search inSPIRE].
[24] M. Pace and J. L. Said, Eur. Phys. J. C **77**, 283 (2017) [arXiv:1704.03343 [gr-qc]] [Search inSPIRE].
[25] M. Krššák and E. N. Saridakis, Classical Quantum Gravity **33**, 115009 (2016) [arXiv:1510.08432 [gr-qc]] [Search inSPIRE].
[26] A. Kolhatkar, S. S. Mishra, and P. K. Sahoo, Eur. Phys. J. C **84**, 888 (2024) [arXiv:2409.01538 [gr-qc]] [Search inSPIRE].
[27] S. S. Mishra, N. S. Kavya, P. K. Sahoo, and V. Venkatesha, Astrophys. J. **981**, 13 (2025).
[28] T. Harko, F. S. N. Lobo, S. Nojiri, and S. D. Odintsov, Phys. Rev. D **84**, 024020 (2011) [arXiv:1104.2669 [gr-qc]] [Search inSPIRE].
[29] S. M. Carroll, V. Duvvuri, M. Trodden, and M. S. Turner, Phys. Rev. D **70**, 043528 (2004) [arXiv:astro-ph/0306438] [Search inSPIRE].
[30] S. Nojiri and S. D. Odintsov, Phys. Rev. D **68**, 123512 (2003) [arXiv:hep-th/0307288] [Search inSPIRE].
[31] A. G. Adame et al. [DESI Collaboration] et al. J. Cosmol. Astropart. Phys. **02** 021 2025 arXiv:2404.03002. [astro-ph.CO] [Search inSPIRE].
[32] G. Alestas, L. Kazantzidis, and S. Nesseris, Phys. Rev. D **106**, 103519 (2022) [arXiv:2209.12799 [astro-ph.CO]] [Search inSPIRE].
[33] L. Kazantzidis and L. Perivolaropoulos, Phys. Rev. D **97**, 103503 (2018) [arXiv:1803.01337 [astro-ph.CO]] [Search inSPIRE].
[34] S. Nesseris, G. Pantazis, and L. Perivolaropoulos, Phys. Rev. D **96**, 023542 (2017) [arXiv:1703.10538 [astro-ph.CO]]] [Search inSPIRE].
[35] A. Królak and P. Verma, Universe **7**, 137 (2021).
[36] B. P. Abbott et al. [LIGO Scientific and Virgo Collaborations], Phys. Rev. X **9**, 031040 (2019) [arXiv:1811.12907 [astro-ph.HE]] [Search inSPIRE].
[37] R. Abbott et al. [LIGO Scientific and Virgo Collaborations], Phys. Rev. X **11**, 021053 (2021) [arXiv:2010.14527 [gr-qc]] [Search inSPIRE].
[38] R. Abbott et al. [LIGO Scientific and Virgo Collaborations], Phys. Rev. D **109**, 022001 (2024) [arXiv:2108.01045 [gr-qc]] [Search inSPIRE].
[39] R. Abbott et al. [KAGRA, Virgo, and LIGO Scientific Collaborations], Phys. Rev. X **13**, 041039 (2023) [arXiv:2111.03606 [gr-qc]] [Search inSPIRE].
[40] R. Jimenez, L. Verde, T. Treu, and D. Stern, Astrophys. J. **593**, 622 (2003) [arXiv:astro-ph/0302560] [Search inSPIRE].
[41] M. Moresco et al., J. Cosmol. Astropart. Phys. **1208**, 006 (2012) [arXiv:1201.3609 [astro-ph.CO]] [Search inSPIRE].
[42] C. Zhang, H. Zhang, S. Yuan, T.-J. Zhang, and Y.-C. Sun, Res. Astron. Astrophys. **14**, 1221 (2014) [arXiv:1207.4541 [astro-ph.CO]] [Search inSPIRE].
[43] D. Stern, R. Jimenez, L. Verde, M. Kamionkowski, and S. A. Stanford, J. Cosmol. Astropart. Phys. **1002**, 008 (2010) [arXiv:0907.3149 [astro-ph.CO]] [Search inSPIRE].
[44] J. Simon, L. Verde, and R. Jimenez, Phys. Rev. D **71**, 123001 (2005) [arXiv:astro-ph/0412269] [Search inSPIRE].
[45] M. Moresco, Mon. Not. R. Astron. Soc. **450**, L16 (2015) [arXiv:1503.01116 [astro-ph.GA]] [Search inSPIRE].
[46] M. Moresco, L. Pozzetti, A. Cimatti, R. Jimenez, C. Maraston, L. Verde, D. Thomas, A. Citro, R. Tojeiro, and D. Wilkinson, J. Cosmol. Astropart. Phys. **1605**, 014 (2016) [arXiv:1601.01701 [astro-ph.CO]] [Search inSPIRE].

[47] A. L. Ratsimbazafy, S. I. Loubser, S. M. Crawford, C. M. Cress, B. A. Bassett, R. C. Nichol, and P. Väisänen, Mon. Not. R. Astron. Soc. **467**, 3239 (2017) [arXiv:1702.00418 [astro-ph.CO]] [Search inSPIRE].
[48] M. Moresco, R. Jimenez, L. Verde, A. Cimatti, and L. Pozzetti, Astrophys. J. **898**, 82 (2020) [arXiv:2003.07362 [astro-ph.GA]] [Search inSPIRE].
[49] D. Rubin et al., arXiv:2311.12098 [astro-ph.CO] [Search inSPIRE].
[50] D. Dutcher et al. [SPT-3G Collaboration], Phys. Rev. D **104**, 022003 (2021) [arXiv:2101.01684 [astro-ph.CO]] [Search inSPIRE].
[51] G. D'Amico, J. Gleyzes, N. Kokron, K. Markovic, L. Senatore, P. Zhang, F. Beutler, and H. Gil-Marín, J. Cosmol. Astropart. Phys. **2005**, 005 (2020) [arXiv:1909.05271 [astro-ph.CO]] [Search in SPIRE].
[52] A. G. Riess et al., Astrophys. J. **934**, L7 (2022) [arXiv:2112.04510 [astro-ph.CO]] [Search inSPIRE].
[53] G. S. Anand, R. B. Tully, L. Rizzi, A. G. Riess, and W. Yuan, Astrophys. J. **932**, 15 (2022) [arXiv:2108.00007 [astro-ph.CO]] [Search inSPIRE].
[54] D. Fernández Arenas, E. Terlevich, R. Terlevich, J. Melnick, R. Chávez, F. Bresolin, E. Telles, M. Plionis, and S. Basilakos, Mon. Not. R. Astron. Soc. **474**, 1250 (2018) [arXiv:1710.05951 [astro-ph.CO]] [Search inSPIRE].
[55] M. Moresco et al., Living Rev. Relativ. **25**, 6 (2022) [arXiv:2201.07241 [astro-ph.CO]] [Search inSPIRE].
[56] S. Birrer et al., Astron. Astrophys. **643**, A165 (2020) [arXiv:2007.02941 [astro-ph.CO]] [Search in SPIRE].
[57] E. J. Baxter and B. D. Sherwin, Mon. Not. R. Astron. Soc. **501**, 1823 (2021) [arXiv:2007.04007 [astro-ph.CO]] [Search inSPIRE].
[58] S. Aiola et al. [ACT Collaboration], J. Cosmol. Astropart. Phys. **2012**, 047 (2020) [arXiv:2007.07288 [astro-ph.CO]] [Search inSPIRE].
[59] M. Asgari et al. [KiDS Collaboration], Astron. Astrophys. **645**, A104 (2021) [arXiv:2007.15633 [astro-ph.CO]] [Search inSPIRE].
[60] T. M. C. Abbott et al. [DES Collaboration], Phys. Rev. D **98**, 043526 (2018) [arXiv:1708.01530 [astro-ph.CO]] [Search inSPIRE].
[61] H. Miyatake, Y. Kobayashi, M. Takada, T. Nishimichi, M. Shirasaki, S. Sugiyama, R. Takahashi, K. Osato, S. More, and Y. Park, Phys. Rev. D **106**, 083519 (2022) [arXiv:2101.00113 [astro-ph.CO]] [Search inSPIRE].
[62] G. F. Lesci et al., Astron. Astrophys. **659**, A88 (2022) [arXiv:2012.12273 [astro-ph.CO]] [Search in SPIRE].
[63] M. Scherer, M. A. Sabogal, R. C. Nunes, and A. De Felice, Phys.Rev.D **112** 043513 2025 arXiv:2504.20664. [astro-ph.CO] [Search inSPIRE]
[64] A. Gomez-Valent and J. Solà Peracaula, Astrophys. J. **975**, 64 (2024) [arXiv:2404.18845 [astro-ph.CO]] [Search inSPIRE].